Journal of Power Sources 240 (2013) 630–635

Contents lists available at SciVerse ScienceDirect

Journal of Power Sources

journal homepage: www.elsevier.com/locate/jpowsour

Platinum-based intermetallic nanotubes with a core–shell structure as highly active and durable catalysts for fuel cell applications

Chunyu Du [a,*], Meng Chen [b], Wengang Wang [b], Qiang Tan [a], Kai Xiong [a], Geping Yin [a]

[a] School of Chemical Engineering and Technology, Harbin Institute of Technology, Harbin 150001, China
[b] School of Chemistry and Materials Science, Harbin Engineering University, Harbin 150080, China

HIGHLIGHTS

- PtCu intermetallic nanotubes with a Pt/PtCu core–shell nanostructure were synthesized by a galvanic replacement approach.
- The PtCu nanotubes exhibit superior catalytic activity toward the electrooxidation of formic acid.
- The PtCu nanotubes are >10 times durable than the conventional Pt/C catalyst.
- Tailored electronic structure and one-dimensional geometry synergistically contribute to the improved performance.

GRAPHICAL ABSTRACT

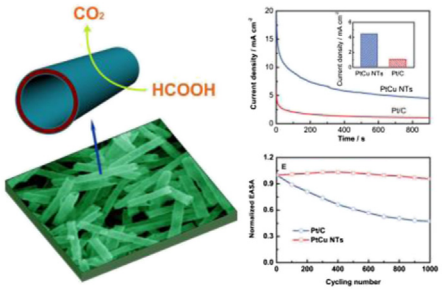

ARTICLE INFO

Article history:
Received 12 March 2013
Received in revised form
3 May 2013
Accepted 8 May 2013
Available online 17 May 2013

Keywords:
Fuel cell catalyst
Platinum–copper nanotube
Core–shell nanostructure
Formic acid oxidation

ABSTRACT

This paper describes the facile synthesis of the PtCu intermetallic nanotubes, which are obtained by a galvanic replacement reaction using Cu nanowires as templates followed by chemical etching and heat annealing. Scanning electron microscopy, X-ray diffraction and X-ray photoelectron spectroscopy are used to characterize the PtCu intermetallic nanotubes. Both cyclic voltammetry and chronoamperometry results demonstrate that these PtCu nanotubes exhibit significantly high catalytic activity toward the formic acid oxidation reaction in comparison with the conventional Pt/C catalyst. Furthermore, the PtCu nanotubes show >10 times higher durability than the Pt/C catalyst in the accelerated ageing test. It is revealed that the PtCu intermetallic nanotubes have a Pt/PtCu core–shell nanostructure that combines the merits of tailorable electronic structures for core–shell nanoparticles and unique geometries for one-dimensional nanotubes, which synergistically contribute to the activity and durability. We believe that the design concept of hierarchy intermetallic nanotubes and the versatile synthetic strategy can not only be used for fuel cell catalysts but also be potentially extended to other catalysis fields.

1. Introduction

Efficient anode catalysts with high activity and durability are critical to the development of direct type fuel cells, such as direct methanol or formic acid fuel cells [1–4]. Unfortunately, the commonly used Pt or Pt alloy nanoparticles (NPs) suffer from the problems of significant CO poisoning (poor activity) and low stability [5,6]. Thus, numerous studies have been conducted to explore alternative high performance anode catalysts. In recent years, nanostructured catalysts have received substantial interests because their unique morphology, composition and structure often lead to greatly improved catalytic activity and

* Corresponding author. Tel.: +86 451 86403216; fax: +86 451 86418616.
E-mail address: cydu@hit.edu.cn (C. Du).

0378-7753/$ – see front matter © 2013 Elsevier B.V. All rights reserved.
http://dx.doi.org/10.1016/j.jpowsour.2013.05.023

stability [7,8]. The nanostructured electrocatalysts reported for fuel cell applications include heterogeneous Pt–Pd nanocomposites [9,10], Pt-based core–shell NPs [11,12], Pt nanocubes or nanopolyhedra [13–15], and Pt nanowires (NWs) or nanotubes (NTs) [16–18]. Among them, Pt-based core–shell NPs show superior catalytic properties, which can be largely attributed to the tailored electronic structure of surface atomic layers by the central cores [19–22]. For example, Pd@Pt and PtNi@Pt core–shell NPs showed over 1 order of magnitude and 5.4 times higher activity for oxygen reduction reaction (ORR) than conventional carbon supported Pt (Pt/C) catalyst, respectively [21,22]. In addition to core–shell NPs, one-dimensional Pt NWs or NTs also exhibit promising catalytic activity and stability, which is closely associated with their anisotropy and unique structures [18,23]. For instance, Sun et al. demonstrated that Pt NWs showed a 2.4-fold higher ORR activity than commercial Pt catalyst [23], while Yan et al. reported that Pt NTs exhibited superior stability as the ORR catalyst [18].

Apparently, the results for core–shell and one-dimensional Pt nanostructures as fuel cell catalysts are intriguing. However, to the best of our knowledge, there is still no effort devoted to the construction of hierarchy Pt nanostructures that combine the merits of core–shell and one-dimensional Pt nanostructures. Besides, present nanostructured electrocatalysts are mostly used for the ORR, and attempts to use them as the anode catalysts are rarely carried out. Herein, we report a novel concept of hierarchy PtCu intermetallic NTs with a Pt/PtCu core–shell nanostructure as an anode catalyst for direct type fuel cells. Our approach integrates the benefits of core–shell NPs and one-dimensional NTs, which would synergically contribute to the catalyst activity and stability. First, the underlying PtCu alloy layer can tailor the electronic structure of surface Pt layers, which thereby, on the one hand, modifies the chemisorption energies and activation barriers for the anode processes, and on the other hand, reduces the Pt dissolution in fuel cell conditions. Second, the interconnected nature renders our hierarchy PtCu NTs less vulnerability to aggregation than Pt NPs. Third, Pt is stable so that the outer Pt surfaces can prevent the etching loss of underlying Cu atoms. Fourth, the PtCu NTs do not require a support, and the support corrosion problem in conventional Pt/C catalyst is thus eliminated. Catalytic properties of the hierarchy PtCu intermetallic NTs were evaluated towards the electrooxidation of small organic molecules for fuel cell applications, and they showed significantly higher activity and stability than the conventional Pt/C catalyst.

2. Experimental section

2.1. Synthesis of Cu NWs

Cu NWs were prepared by an electrodepositing method. An anodic alumina film (Whatman, Anodisc 25) with a nominal pore size of 200 nm was used as the template for the electrodeposition. A 500-nm-thick Cu film evaporated onto one side of the template served as the working electrode in a three-electrode cell with a Pt mesh as the counter electrode and an Hg/Hg_2SO_4 electrode as the reference electrode, respectively. Cu NWs approximately 20 μm long were deposited from a solution containing 0.1 M $CuSO_4$, 0.1 M H_3BO_3 and 25 mg L^{-1} polyethylene glycol at −0.6 V (vs. Hg/Hg_2SO_4). After deposition, the Cu film was stripped by etching in a solution of 0.3 M $CuCl_2$ and 0.1 M HCl. The alumina template was then dissolved in 2.0 M NaOH for 2 h, and the remaining Cu NWs were centrifuged, washed thoroughly, and suspended in N_2-saturated deionized water containing 8.0 mM poly(vinyl pyrrolidone).

2.2. Synthesis of PtCu intermetallic NTs

The PtCu intermetallic NTs were synthesized by a galvanic replacement reaction followed by chemical dealloying and heat annealing processes. In a typical synthesis, the solution containing Cu NWs was heated to 80 °C. Subsequently, 0.5 mM H_2PtCl_6 aqueous solution was added. After the mixture was vigorously stirred for >30 min, the resulting PtCu alloy sheathed Cu NWs were separated and washed with deionized water. The chemical dealloying treatment was performed by immersing the sheathed Cu NWs into 10 wt% NH_3 solution for 2 h. The samples were then filtered and washed by deionized water and ethanol to obtain the hierarchy PtCu NTs. The heat annealing was carried out under an $Ar–H_2$ flow (5% H_2) in a tube-oven at 500 °C for 3 h.

2.3. Physical characterization of PtCu intermetallic NTs

Scanning electron microscopy (SEM) was carried out on an FEI Quanta 200FEG instrument equipped with an energy dispersion X-ray spectroscopy (EDX) device (10 kV). X-ray diffraction (XRD) patterns were collected on a Rigaku D/MAX-3B diffractometer with Cu Kα radiation. Transmission electron microscopy (TEM) was conducted on a Hitachi H800 system (200 kV). X-ray photoelectron spectroscopy (XPS) was performed on a PHI model 5700 spectrometer using Al Kα X-ray source.

2.4. Electrochemical treatment and tests

Electrochemical treatment and tests of the PtCu intermetallic NTs were performed on a rotating disk electrode (RDE) apparatus (Princeton Applied Research) in a three-compartment electrochemical cell with a Pt foil and an Hg/Hg_2SO_4 electrode serving as the counter and reference electrodes, respectively. Prior to each experiment, a suspension of the PtCu NTs was prepared as follows: To 3.5 mg dried PtCu NTs, 2.7 mL deionized water, 0.725 mL isopropanol and 0.075 mL Nafion solution (5%) were added; The resulting mixture was sonicated for 30 min to form homogeneous suspension. 12.5 μl of the suspension was coated onto a glassy carbon RDE electrode (4 mm diameter), which was then dried at 50 °C under a N_2 atmosphere for 30 min to serve as the working electrode.

Before electrochemical tests, a pretreatment of the working electrodes was performed by potentially cycling them between 0.05 and 1.2 V for 50 cycles at a scan rate of 50 mV s^{-1} in 0.5 M H_2SO_4 solution. Cyclic voltammetry (CV) measurements for formic acid oxidation were carried out in a N_2-saturated 0.5 M H_2SO_4 solution containing 0.5 M HCOOH at a scan rate of 50 mV s^{-1} in the range of 0.05–1.2 V. Chronoamperommetry (CA) tests were conducted by holding the working electrode at 0.4 V in a solution of 0.5 M H_2SO_4 and 0.5 M HCOOH. Electrochemically active surface area (EASA) of the samples was evaluated by the H_2 desorption peak in the CV profiles obtained in a N_2-saturated 0.5 M H_2SO_4 solution at a scan rate of 50 mV s^{-1}. For CO-stripping measurements, the working electrode was firstly poisoned with CO at 0.1 V by bubbling CO gas through 0.5 M H_2SO_4 aqueous solution for 30 min. Linear sweeping voltammetry was then conducted at a scan rate of 10 mV s^{-1} after the remaining CO in the electrolyte solution was removed by purging N_2 for 40 min. All electrochemical experiments were carried out at room temperature and all potentials in this study are given relative to the reversible hydrogen electrode (RHE). For the sake of comparison, the Pt/C catalyst was also synthesized (see Supplementary material for details) and tested.

3. Results and discussion

3.1. Synthesis of the PtCu intermetallic NTs

We employ a galvanic replacement reaction followed by chemical dealloying and heat annealing processes to synthesize the PtCu intermetallic NTs. Fig. 1A shows a schematic illustration of the synthesis procedure. The first step involves the electrodeposition of Cu NWs with a porous alumina film as the template. After removal of the template, the Cu NWs galvanically react with platinate to deposit PtCu alloy sheaths on Cu NWs. Subsequently, most of Cu is chemically etched away to form the PtCu NTs. The PtCu NTs are finally subject to heat treatment under a reducing atmosphere. Fig. 1B presents a typical SEM image of as-prepared Cu NWs, which exhibit uniform wire shapes with average size of ~245 nm in diameter, roughly consistent with the pore diameter of the alumina template used. After the galvanic replacement reaction (Fig. 1C), the mean diameter of Cu NWs is increased to ~288 nm, indicating that Pt has been successfully deposited on the surface of Cu NWs. According to previous studies on galvanic replacement reactions [24], we believe that the deposited Pt atoms tend to alloy with Cu atoms, leading to the formation of PtCu alloy sheath. Note that each NW after Pt sheathing is still straight and uniform in diameter along the entire axis, suggesting that the PtCu alloy sheaths are even. It can also be observed from Fig. 1C that some surfaces of the Cu NWs are decorated with small particles (indicated by rectangles), which might be ascribed to the poor expitaxial growth of Pt on Cu surface as a result of the relatively large difference in lattice constants between Pt and Cu metals [25]. The PtCu alloy sheathed Cu NWs are analyzed by EDX to be composed of 89.4 mol% Cu and 10.6 mol% Pt, respectively. When most of Cu is removed from the sheathed Cu NWs by chemical dealloying, the product is clearly characterized by a tubular structure with wall thickness of ~20 nm (Fig. 1D), and contains 48.6 mol% of Pt as revealed by EDX. In order to eliminate the remaining surfactant and form the PtCu intermetallic phase, the PtCu NTs are heat-treated at 500 °C under a reducing atmosphere. After heating (Fig. 1E), the long PtCu NTs break down into shorter

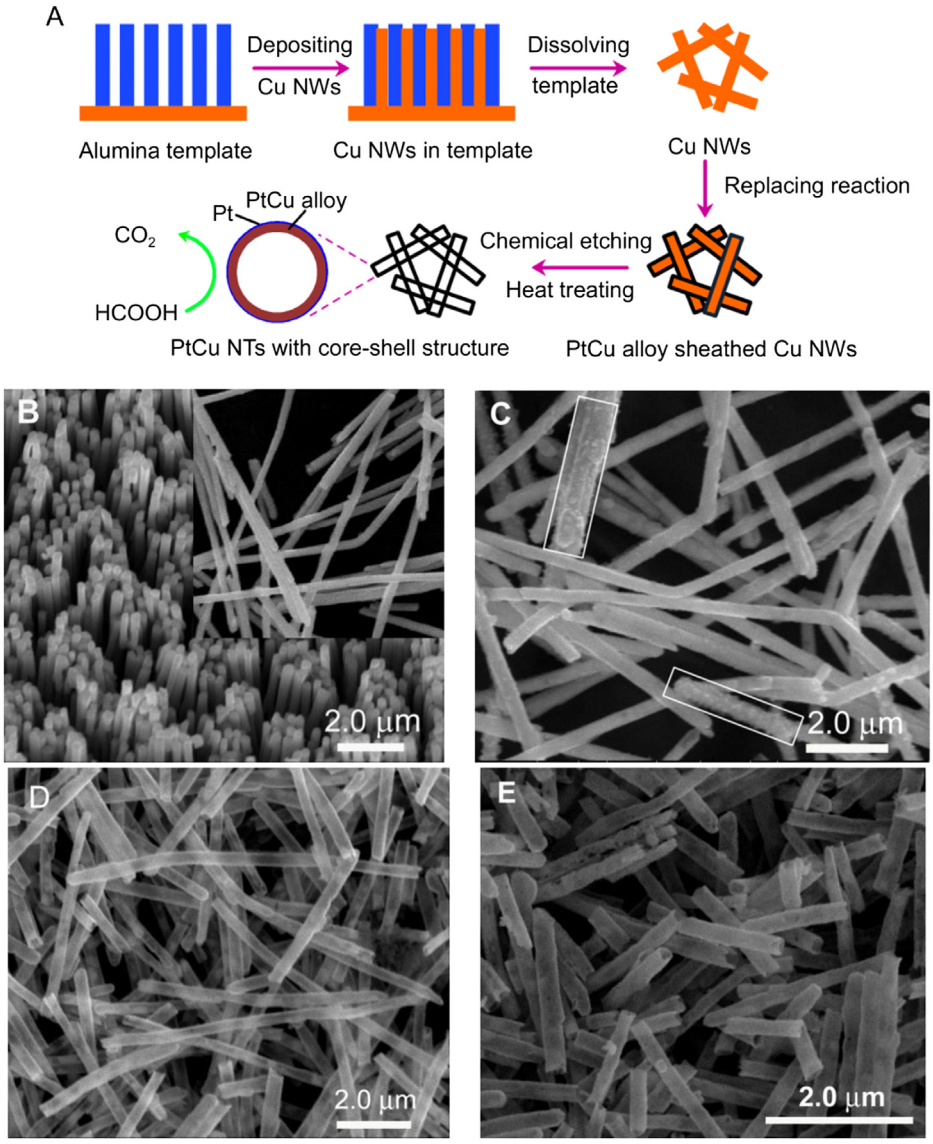

Fig. 1. (A) Schematic illustration of the synthesis of PtCu NTs, and SEM images of Cu NWs (B), PtCu alloy sheathed Cu NWs (C), chemically etched PtCu NTs (D) and heat-treated PtCu NTs (E).

ones to release the thermal stress during the heat-treatment process. Also, a small part of the NT surfaces are a little rough and contain nano-pinholes, which is probably due to the chemical etching and the poor expitaxial growth of Pt on Cu as mentioned above. This roughness will lead to higher active surface area, contributing positively to the activity of the PtCu intermetallic NTs.

Structural characterization of the synthesis of the PtCu intermetallic NTs is carried out using XRD (Fig. 2A). The electrodeposited Cu NWs clearly show a reflection profile consistent with a face-centered cubic crystal symmetry of Cu (JCPDS-04-0836). After the replacement reaction, the diffraction pattern of the sheathed Cu NWs presents additional peaks at angles higher than pure Pt, confirming that PtCu alloy sheath instead of pure Pt is formed. Chemical etching of the sheathed Cu NWs eliminates the diffraction peaks for Cu as expected, indicating the formation of PtCu NTs. Further heat annealing of the PtCu NTs increases the crystallinity of PtCu alloy, leading to the enhancement of the peak intensities and the formation of PtCu intermetallic phase.

Information on chemical states of the PtCu intermetallic NTs is obtained by XPS. From the wide survey spectrum (Fig. S1 in Supplementary material), the presence of Pt in the PtCu NTs is clearly confirmed. Meanwhile, weak peaks for Cu are observed (evidenced by the detailed Cu 2p spectrum in Fig. S2 of Supplementary material). The composition of the surface of PtCu intermetallic NTs is $Pt_{88}Cu_{12}$, which is different from that of bulk material ($Pt_{49}Cu_{51}$), indicating that there is Pt enrichment or aggregation on the surface of PtCu intermetallic NTs, which has been observed and confirmed on Pt-based alloys by the previous study [26]. It should be noted that the enriched Pt layer on the surface of PtCu intermetallic NTs is not resolved by the XRD pattern, which might be due to the fact that the Pt surfaces are rather thin, consistent with previous studies [27,28]. To carry out in-depth analyses, detailed XPS scans of the Pt 4f region for the PtCu intermetallic NTs and Pt/C catalyst are acquired (Fig. 2B). The Pt 4f spectra are deconvoluted into two doublets assigned to metallic Pt and oxidized Pt in the divalent state, respectively. Comparison of the relative areas of corresponding doublets reveals that Pt in the PtCu NTs possesses less amount of oxidized states than that in Pt/C (21.9 mol% for PtCu NTs vs. 32.8 mol% for Pt/C), suggesting that the PtCu intermetallic NTs have a lower chemical adsorption energy with oxygen. Furthermore, the Pt 4f electron binding energy for the PtCu NTs is significantly shifted to lower values relative to the Pt/C, mainly due to the partial electron transfer from the Cu atoms to the Pt atoms. Such a decrease in binding energy reflects the downshift of d-band center of Pt atoms, which will lead to the weakened chemisorption of oxygen-containing species such as CO_{ads} and OH_{ads} on Pt surface and contribute positively to the catalyst activity or stability [29–31].

3.2. Electrochemical performance of the hierarchy PtCu NTs

Although Pd-based electrocatalysts are highly active towards the reaction of formic acid oxidation (FAO), they show rather low long-term stability in the corrosive formic acid solutions [32–34]. Thus, Pt-based nanomaterials are the most promising and desirable FAO catalysts [35]. In order to promote the formation of Pt skin layer on the surface of PtCu intermetallic NTs and render the PtCu NTs electrochemically active, the PtCu NTs were firstly treated by potentially cycling between 0.05 and 1.2 V at a scan rate of 50 mV s^{-1} in 0.5 M H_2SO_4 solution. It is well known that Pt-based metal alloys usually exhibit the formation of a Pt skin after electrochemical cycling in acidic electrolytes, which is mainly caused by electrochemical dissolution of the less noble component from the alloy accompanied by regrouping of Pt atoms [36,37]. From the steady-state CV curves of the catalysts in 0.5 M H_2SO_4 solution (Fig. S3 in Supplementary material), it can be seen that the voltammetric features of the PtCu intermetallic NTs are similar to those at a Pt/C catalyst, suggesting the formation of a Pt skin on the surface of PtCu intermetallic NTs after electrochemical treatment [37].

Electrocatalytic activity of the PtCu intermetallic NTs towards the FAO reaction is evaluated by CV and CA in a 0.5 M H_2SO_4 solution containing 0.5 M HCOOH. For the CV curves (Fig. 3A), during the positive scan, the current plateau between 0.4 and 0.8 V is assigned to the direct oxidation of formic acid to CO_2 (direct path), while the current peak at ~0.88 V corresponds to the oxidation of the poisoning intermediates (usually CO) accumulated during the dehydration of formic acid (CO path) [37–40]. Therefore, the ratio between the plateau and the peak reveals the relatively favourable path during the FAO process. It is observed that the current plateau for the PtCu NTs is more than 17 times higher than that for the Pt/C. Furthermore, the PtCu NTs present a plateau/peak ratio of 0.82, which means a 3.4-fold improvement from the Pt/C. These observations clearly indicate that the PtCu NTs are highly active for the FAO.

CA profiles of the PtCu NTs and Pt/C are recorded with a bias at 0.4 V (Fig. 3B). Both the transient FAO currents decay with time and reach an apparent steady-state after 15 min. However, the current attenuation for the PtCu NTs takes a much longer time. Moreover, the steady-state current density for the PtCu NTs is 4.2 times larger than that for the Pt/C, which is consistent with the CV results and indicates that the PtCu NTs have a higher steady-state activity towards the FAO reaction.

The enhanced activity of the PtCu intermetallic NTs is mainly attributed to the tailored electronic structure of the surface Pt layers by the underlying PtCu layer. As revealed by XPS results, there is some electron transfer from the underlying PtCu layer to

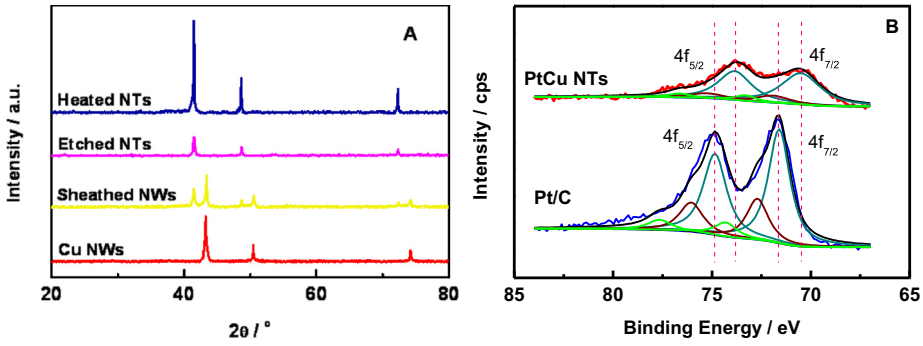

Fig. 2. (A) XRD patterns of the Cu NWs, PtCu alloy sheathed Cu NWs, PtCu NTs by chemical etching and heat-treated PtCu NTs, and (B) detailed Pt 4f XPS spectra of the hierarchy PtCu NTs and Pt/C catalyst.

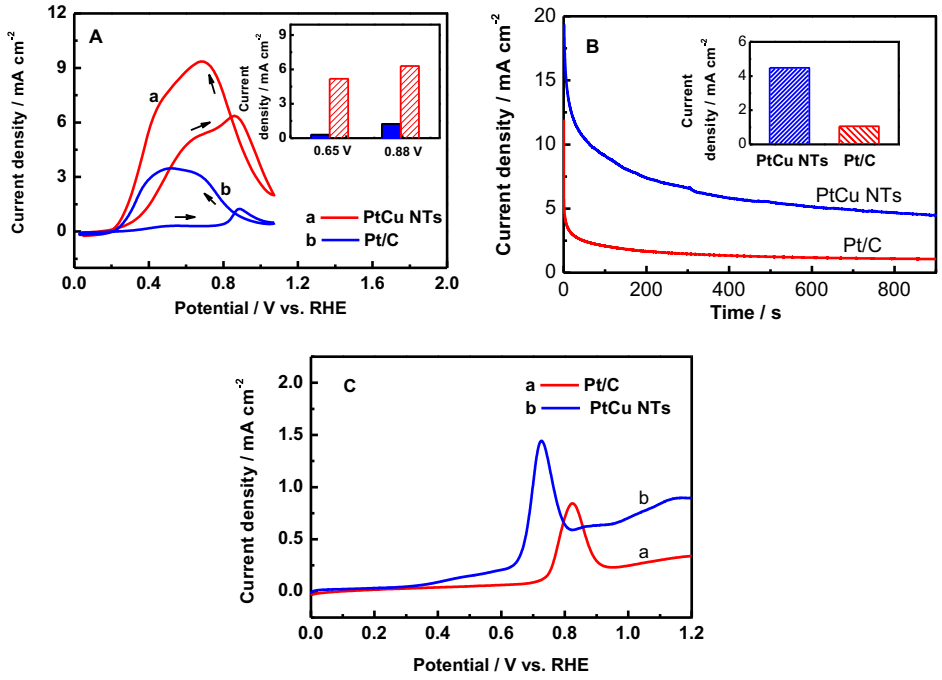

Fig. 3. (A) CV curves (inset: activity comparison during the positive scan) and (B) CA curves (inset: steady-state activities after 15 min of polarization) of the hierarchy PtCu NTs and the Pt/C in 0.5 M H_2SO_4 and 0.5 M HCOOH solution, and (C) CO-stripping voltammetric curves for the PtCu NTs and Pt/C recorded in 0.5 M H_2SO_4 solution at a scan rate of 10 mV s^{-1}.

the Pt surface layer, which will weaken the binding strength of the absorbed intermediates (usually CO) on the PtCu NTs, and lead to improved electrocatalytic activity. This inference is clearly verified by the CO-stripping voltammetry for the PtCu NTs and the Pt/C catalyst (Fig. 3C). The PtCu NTs exhibit significant decrease in the onset and peak potentials for CO-stripping in comparison with the Pt/C catalyst, clearly indicating that the PtCu NTs facilitate the electrooxidation of CO poisoning intermediate [41].

Durability of the PtCu NTs as an FAO catalyst is acceleratedly investigated by repeatedly cycling them between 0 and 1.2 V in 0.5 M H_2SO_4 and 0.5 M HCOOH solution (Fig. S4 in Supplementary material). After 1000 cycles, the Pt/C catalyst shows a significant activity degradation, which remains 60.3% and 58.2% of its initial activity for the direct and CO paths, respectively (Fig. 4A). In contrast, the PtCu NTs present only a slight activity decrease after the same test (Fig. 4B). The much higher FAO durability of our PtCu

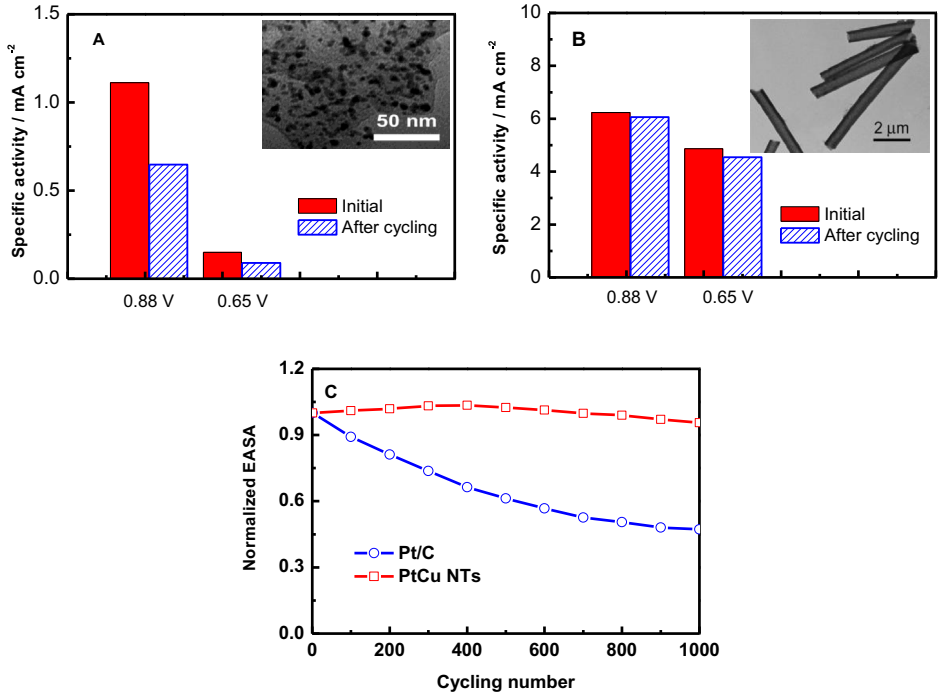

Fig. 4. Electrochemical stability of the direct and CO paths for the Pt/C (A) and hierarchy PtCu bimetallic NTs (B) in 0.5 M H_2SO_4 and 0.5 M HCOOH solution at a scan rate of 50 mV s^{-1} (inset: TEM images of the catalysts after the durability tests), and (C) evolution of the normalized EASA for the PtCu NTs and Pt/C in 0.5 M H_2SO_4 solution.

NTs can be attributed to their stable nanostructures, in addition to the high poisoning-resistance as revealed by the CO-stripping curves. TEM observation reveals that the average size of Pt NPs in the Pt/C catalyst increases significantly from original 2.9 nm (Fig. S5 in Supplementary material) to 8.5 nm after the durability test (inset of Fig. 4A). However, there are no noticeable morphological changes for the PtCu NTs (inset of Fig. 4B). Structural stability of the PtCu NTs is further confirmed by their EASA shown in Fig. 4C, which is calculated from the H-desorption peaks for the CV curves measured in H_2SO_4 solution and normalized by their initial EASA values (Figs. S3 and S6 in Supplementary material). After 1000 cycles, EASA of the PtCu NTs decreases about 4.5%, while the Pt/C has lost about 52.3% of its initial EASA, consistent with the TEM observations. We believe that the structural stability of the PtCu NTs is closely related to their tubular morphology and core–shell nanostructure. It has been proven that the instability of Pt NPs in fuel cell environments can be ascribed to their aggregation, dissolution, and electrical discontact due to the support corrosion [42,43]. Our PtCu NTs prolong their stability by simultaneously alleviating these degradation pathways. First, the interconnected nature of the PtCu NTs significantly reduces the aggregation problem common for Pt NPs [18]. Second, the PtCu NTs do not require a support, and thus the support corrosion problem is completely eliminated. Third, the outer Pt surface is electronically modulated by the underlying PtCu alloy layer, which weakens the chemisorption of oxygen-containing species, making the PtCu NTs more electrooxidation resistant [29,30]. This resistance is apparently verified by the higher oxidation potential for the PtCu NTs (Fig. S7 in Supplementary material), which will lead the PtCu NTs to be less vulnerable to Pt dissolution because the formation of Pt oxides contributes significantly to Pt dissolution [44]. These facts clearly explain the excellent structural stability of our PtCu intermetallic NTs with a core–shell nanostructure, enabling their potential use as a highly durable catalyst for FAO and other fuel cell anode reactions.

4. Conclusion

In conclusion, we have described the facile preparation of the hierarchy PtCu intermetallic NTs with a Pt/PtCu core–shell nanostructure, which result from first electrodepositing Cu NWs within alumina pores, subsequent coating a PtCu alloy sheath by a galvanic replacement reaction, chemical etching and heat annealing, and final electrochemical dealloying. This procedure provides a versatile route to a unique hierarchy metallic nanostructure with tubular and core–shell features. By judiciously choosing the galvanic replacement system, the diameter, composition and surface chemistry of the hierarchy nanostructure can be well controlled. The hierarchy nanostructure delicately combines the merits of tailorable electronic structures for core–shell NPs and unique geometries for metallic NTs. Therefore, the obtained PtCu bimetallic NTs exhibit superior catalytic activity (>4 times more active than Pt/C) and rather high durability (>10 times more durable than Pt/C) toward the reaction of FAO. We believe that the concept of hierarchically combined tubular and core–shell nanostructures as well as the fabrication technique can be not only used for fuel cell catalysts but also potentially extended to other fields, such as electrochemical sensing and photo-electrochemistry.

Acknowledgements

This work was supported by the National Science Foundation of China under contract Nos. 20706010 and 20876029, and the Harbin Talents Foundation in the Innovation of Science and Technology (2008RFQXG059).

Appendix A. Supplementary data

Supplementary data related to this article can be found at http://dx.doi.org/10.1016/j.jpowsour.2013.05.023.

References

[1] X. Yu, P.G. Pickup, J. Power Sources 192 (2009) 279–284.
[2] X. Zhao, M. Yin, L. Ma, L. Liang, C.P. Liu, J.H. Liao, T.H. Lu, W. Xing, Energy Environ. Sci. 4 (2011) 2736–2753.
[3] C. Rice, S. Ha, R.I. Masel, P. Waszczuk, A. Wieckowski, T. Barnard, J. Power Sources 111 (2002) 83–89.
[4] C. Rice, S. Ha, R.I. Masel, A. Wieckowski, J. Power Sources 115 (2003) 229–235.
[5] H. Ren, M.P. Humbert, C.A. Menning, J.G. Chen, Y. Shu, U.G. Singh, W. Cheng, Appl. Catal. A-Gen. 375 (2010) 303–309.
[6] X. Yu, S. Ye, J. Power Sources 172 (2007) 145–154.
[7] B. Wickman, Y.E. Seidel, Z. Jusys, B. Kasemo, R.J. Behm, ACS Nano 5 (2011) 2547–2558.
[8] J. Wu, A. Gross, H. Yang, Nano Lett. 11 (2011) 798–802.
[9] Z. Peng, H. Yang, J. Am. Chem. Soc. 131 (2009) 7542–7543.
[10] B. Lim, M. Jiang, P.H.C. Camargo, E.C. Cho, J. Tao, X. Lu, Y. Zhu, Y. Xia, Science 324 (2009) 1302–1305.
[11] K. Sasaki, H. Naohara, Y. Cai, Y.M. Choi, P. Liu, M.B. Vukmirovic, J.X. Wang, R.R. Adzic, Angew. Chem. Int. Ed. 49 (2010) 8602–8607.
[12] Y. Kang, L. Qi, M. Li, R. Diaz, D. Su, R. Adzic, E. Stach, J. Li, C. Murray, ACS Nano 6 (2012) 2818–2825.
[13] C. Wang, H. Daimon, Y. Lee, J. Kim, S. Sun, J. Am. Chem. Soc. 129 (2007) 6974–6975.
[14] C. Wang, H. Daimon, T. Onodera, T. Koda, S. Sun, Angew. Chem. Int. Ed. 47 (2008) 3588–3591.
[15] Y. Kang, C. Murray, J. Am. Chem. Soc. 132 (2012) 7568–7569.
[16] E.P. Lee, Z. Peng, W. Chen, S. Chen, H. Yang, Y. Xia, ACS Nano 2 (2008) 2167–2173.
[17] S. Sun, G. Zhang, D. Geng, Y. Chen, R. Li, M. Cai, X. Sun, Angew. Chem. Int. Ed. 50 (2011) 422–426.
[18] Z. Chen, M. Waje, W. Li, Y. Yan, Angew. Chem. Int. Ed. 46 (2007) 4060–4063.
[19] S. Koh, P. Strasser, J. Am. Chem. Soc. 129 (2007) 12624–12625.
[20] T.-Y. Jeon, K.-S. Lee, S.J. Yoo, Y.-H. Cho, S.H. Kang, Y.-E. Sung, Langmuir 26 (2010) 9123–9129.
[21] C. Wang, D. van der Vliet, K.L. More, Nano Lett. 11 (2011) 919–926.
[22] W. Li, P. Haldara, Electrochem. Solid-State Lett. 13 (2010) B47–B49.
[23] S. Sun, G. Zhang, D. Geng, Y. Chen, R. Li, M. Cai, X. Sun, Chem. Eur. J. 16 (2010) 829–835.
[24] Y. Sun, Z. Tao, J. Chen, T. Herricks, Y. Xia, J. Am. Chem. Soc. 126 (2004) 5940–5941.
[25] Y. Sun, Y. Xia, J. Am. Chem. Soc. 126 (2004) 3892–3901.
[26] C. Wang, M. Chi, D. Li, D. Strmcnik, D. van der Vliet, G. Wang, V. Komanicky, K.-C. Chang, A.P. Paulikas, D. Tripkovic, J. Pearson, K.L. More, N.M. Markovic, V.R. Stamenkovic, J. Am. Chem. Soc. 133 (2011) 14396–14403.
[27] P. Mani, R. Srivastava, P. Strasser, J. Phys. Chem. C 112 (2008) 2770–2778.
[28] I. Dutta, M.K. Carpenter, M.P. Balogh, J.M. Ziegelbauer, T.E. Moylan, M.H. Atwan, N.P. Irish, J. Phys. Chem. C 114 (2010) 16309–16320.
[29] S. Wang, S.P. Jiang, X. Wang, J. Guo, Electrochim. Acta 56 (2011) 1563–1569.
[30] F. Lima, J. Zhang, M. Shao, K. Sasaki, M. Vukmirovic, E.A. Ticianelli, R.R. Adzic, J. Phys. Chem. C 111 (2007) 404–410.
[31] M. Mavrikakis, B. Hammer, J.K. Norskov, Phys. Rev. Lett. 81 (1998) 2819–2822.
[32] W.P. Zhou, A. Lewera, R. Larsen, R.I. Masel, P.S. Bagus, A. Wieckowski, J. Phys. Chem. B 110 (2006) 13393–13398.
[33] J.J. Ge, Y.W. Zhang, C.P. Liu, T.H. Lu, J.H. Liao, W. Xing, J. Phys. Chem. C 112 (2008) 17214–17218.
[34] J.Y. Wang, Y.Y. Kang, H. Yang, W.B. Cai, J. Phys. Chem. C 113 (2009) 8366–8378.
[35] D. Chen, Z. Zhou, Q. Wang, D. Xiang, N. Tian, S. Sun, Chem. Commun. 46 (2010) 4252–4254.
[36] W. Chen, J. Kim, L.-P. Xu, S. Sun, S. Chen, J. Phys. Chem. C 111 (2007) 13452–13459.
[37] W. Chen, J. Kim, S. Sun, S. Chen, Langmuir 23 (2007) 11303–11310.
[38] W. Chen, J. Kim, S. Sun, S. Chen, Phys. Chem. Chem. Phys. 8 (2006) 2779–2786.
[39] X. Ji, K. Lee, R. Holden, L. Zhang, J. Zhang, G.A. Botton, M. Couillard, L.F. Nazar, Nat. Chem. 2 (2010) 286–293.
[40] N. Marković, H. Gasteiger, P. Ross, Electrochim. Acta 40 (1995) 91–98.
[41] H. Gasteiger, N. Marković, P. Ross, J. Phys. Chem. 99 (1995) 8290–8301.
[42] R. Borup, J. Meyers, B. Pivovar, Y. Kim, R. Mukundan, N. Garland, D. Myers, M. Wilson, F. Garzon, D. Wood, P. Zelenay, K. More, K. Stroh, T. Zawodzinski, X. Boncella, J.E. McGrath, O. Inaba, K. Miyatake, M. Hori, K. Ota, Z. Ogumi, S. Miyata, A. Nishikata, Z. Siroma, Y. Uchimoto, K. Yasuda, K. Kimijima, N. Iwashita, Chem. Rev. 107 (2007) 3904–3951.
[43] J. Wu, X.Z. Yuan, J.J. Martin, H. Wang, J. Zhang, J. Shen, S. Wu, W. Merida, J. Power Sources 184 (2008) 104–119.
[44] P. Ferreira, G. La O', Y. ShaoHorn, D. Morgan, R. Makharia, S. Kocha, H. Gasteiger, J. Electrochem. Soc. 152 (2005) A2256–A2271.